Atmospheric Environment 215 (2019) 116874

Contents lists available at ScienceDirect

Atmospheric Environment

journal homepage: www.elsevier.com/locate/atmosenv

Surveillance efficiency evaluation of air quality monitoring networks for air pollution episodes in industrial parks: Pollution detection and source identification

Zihan Huang[a], Qi Yu[a,b,c,**], Weichun Ma[a,b,c], Limin Chen[a,*]

[a] Department of Environmental Science and Engineering, Fudan University, Shanghai, 200438, China
[b] Big Data Institute for Carbon Emission and Environmental Pollution, Fudan University, Shanghai, 200433, China
[c] Shanghai Institute of Eco-Chongming (SIEC), No.3663 Northern Zhongshan Road, Shanghai, 200062, China

ARTICLE INFO

Keywords:
Air pollition episodes
Boundary-type monitoring network
Gaussian puff model
Source area analysis
Hydrogen sulfide

ABSTRACT

Both air pollution detection and source identification for air pollution episodes are highly desirable for detecting and controlling industrial air pollution. Surveillance of air pollution episodes in industrial parks is the focus of this article. The surveillance in this study consists of air pollution detection and subsequent source identification. The Gaussian puff model is applied to simulate the dispersion of air pollution, and the source area analysis method is used to reconstruct unknown source terms. A case study involving hydrogen sulfide emissions in a typical chemical industrial park is presented. The long-term efficiencies of both pollution detection and source identification of a developing planning of boundary-type air quality monitoring network (AQMN) are evaluated. Five typical scenarios are identified for the evaluation. Moreover, several key factors for the surveillance efficiency variation (*i.e.,* meteorological conditions, monitor number and distance between sources) are discussed. The efficiency of pollution detection increases with the number of monitors. The efficiency of source identification increases with the number of monitors and the distance between sources.

1. Introduction

Recently, source identification for environmental air pollution has become a major research topic. The primary mission of AQMNs deployed in industrial parks or nearby regions is to survey industrial emissions, especially to detect violations over prescribed thresholds (Adams and Kanaroglou, 2013). Violations detected can be used as the input measurements for backward systems to reconstruct emission source terms. Measurements collected by deployed AQMNs have been increasingly employed to reconstruct the unknown source characteristics of air pollution (Khlaifi et al., 2009; Sharan et al., 2012; Cai et al., 2013; Turbelin et al., 2014; Hosseini and Stockie, 2016; Singh et al., 2017; Efthimiou et al., 2017). The results of source inversion can help diminish the contaminant threat and can be used as basic input data for forward dispersion models to predict subsequent transport and dispersion.

However, emission sources are difficult to be reconstructed in many air pollution episodes because of the limited available measurements. Relatively little research has focused on pollution detection and source identification together for air pollution in industrial parks. The surveillance efficiency for air pollution episodes in a chemical industrial park was concerned in this study. The surveillance here referred to pollution detection and subsequent source identification. The time scale of the evaluation was one year to consider the variation of surveillance efficiency with meteorological conditions.

Many AQMNs began operation as a small number of monitors instead of as a well-designed sound systems (Pope and Wu, 2014). The AQMN concerned in this case study distributed along the boundary of the industrial park. Two existing monitoring stations were located near the north-northeast and the east-northeast boundary respectively. It was designed to cover the boundary evenly on 16 wind directions. This layout mode of monitoring network is to monitor the transportation pollution from the inside out with maximum efficiency, which is the typical development pattern in industrial parks.

The full scale of the AQMN in this study was sufficient to detect air pollutant export from the industrial park. However, such network was still too sparse to enable precise source identification. Much more monitors might be required according to the literature. Allen et al. (2007) and Haupt et al. (2007) found that an 8-by-8 grid of monitors is

* Corresponding author.
** Corresponding author. Department of Environmental Science and Engineering, Fudan University, Shanghai, 200438, China.
E-mail addresses: 15110740006@fudan.edu.cn (Z. Huang), qiyu@fudan.edu.cn (Q. Yu), wcma@fudan.edu.cn (W. Ma), lmchen@fudan.edu.cn (L. Chen).

https://doi.org/10.1016/j.atmosenv.2019.116874
Received 9 July 2018; Received in revised form 16 April 2019; Accepted 29 July 2019
Available online 29 July 2019

the minimum needed to reconstruct the source terms (*i.e.,* source location, source strength, and wind direction). Rudd et al. (2012) found that a reasonable estimation of source strength and location could be obtained with as few as four sensors if they were well placed and the sampling error was controlled. The number of monitors for source identification was recommended to be higher than that of the unknowns (Rudd et al., 2012; Singh and Rani, 2014; Singh et al., 2015) due to uncertainties (caused by the lack of a priori information on source parameters, model representativeness errors, limited and noisy concentration information, etc.). Thus, it is worth examining how supportive the AQMN developing program can be for pollution detection and source identification in this industrial park.

Dispersion model is used here to simulate the capture process by AQMN of air pollutant, which is also used to evaluate the efficiency of source identification. Simulated concentrations obtained by a dispersion model were used as ambient concentration measurements because the selected monitoring stations were under construction. Different types of dispersion models can be applied for forward dispersion modelling in source reconstruction. For instance, Flesch et al. (2005) presented a Lagrangian stochastic model for deducing ground-to-air emissions. Ma et al. (2013) adopted a Gaussian plume model to reconstruct a continuous source and explore the performances of different optimization methods for source estimation. Further, a Gaussian-MLA model was proposed by Ma and Zhang (2016) as the forward model to improve the estimation performance in the emission source terms identification. Long et al. (2010) and Rodriguez et al. (2011) employed a Gaussian puff model to simulate the dispersion of instantaneous releases for source determination. An integrated Lagrangian puff model was used by Najafi and Gilbert (2003) for narrowing the possible source locations and estimating the source rate necessary for emergency response. Computational fluid dynamics (CFD) has been combined with source estimation method in urban environment, which included true geometric and flow complexity inherent (Chow et al., 2008; Kovalets et al., 2011; Kumar et al., 2015, 2016; Efthimiou et al., 2017). Gaussian puff model was used in this study as the dispersion model to simulate the concentration distribution of unexpected pollution episodes, because its simplicity (input parameters are available easily), computationally efficient and capability in the unsteady emissions and wind conditions simulation were considered. In addition, pollution episodes are always caused by abnormal emissions, little priori source information was usually available to ensure the operation of explicit dispersion models like CFD and Lagrangian stochastic model. Detailed historical case data have not been accumulated to support the operation of the refined dispersion model in this park. It is uncertain whether the results simulated by refined models are more accurate than those by Gaussian puff model in the absence of detailed prior information of emission source and environmental conditions. Thus we did not use a refined method as the forward model.

Source identification method based on dispersion model was employed in the evaluation of surveillance efficiency. Since the concerned AQMN is sparse, the back-calculation method we used is the source area analysis method developed in our previous work. Source area analysis method was proposed to perform the back-calculation with a limited number of monitoring stations (Huang et al., 2015). In the evaluation process of this work, the source area analysis method described in Huang et al. (2015) was employed to provide a collection of potential source locations for back-calculation under different meteorological conditions. The source area analysis method was proposed to back-calculate source locations with limited monitors and considered the variations in other unknown parameters, such as source strength, source height, release time and release duration. The real source location may not be obtained by source area analysis when prior source information is limited, while a finite range of emission sources distributions can be provided.

The obtained solutions were found to cluster in a fan-shaped area if only one monitor was available in the back-calculation; in other words, any source located in this source area could be the emission source. However, the reconstructed source area in the 2-monitor case was smaller than that obtained in the 1-monitor case. The source area might include some other suspected sources (*i.e.,* fake sources) as well as the real source, so the number of fake sources inside the source area was then counted to denote the efficiency of source identification in surveillance efficiency evaluation.

The remainder of this paper is organized as follows. Section 2 describes the evaluation indexes of surveillance efficiency and the corresponding calculation method. Section 3 introduces typical scenarios of pollution detection efficiency evaluation firstly. The number of monitors that can capture the pollution episodes is different in these scenarios, which affects further available data and results of subsequent source identification evaluation. Then the efficiency evaluation results of pollution detection and source identification are analysed respectively. Moreover, several key factors for surveillance efficiency variation (*i.e.*, meteorological conditions, monitor number and distance between sources) are discussed. A test case is added to analyse the influence of distance between sources on source identification efficiency. Finally the conclusions are given in Section 4.

2. Methods

2.1. Surveillance efficiency evaluation

The main goal of surveillance efficiency evaluation is to quantify the long-term capability of an AQMN to support both air pollution detection and source identification in an industrial park.

r_d is the annual accumulative probability of detecting violations over the air quality ambient standards, and is defined in Equation (1):

$$r_d = \sum_{i=1}^{I} r_{d,i} \tag{1}$$

$$r_{d,i} = \sum_{m=1}^{M} P_m T_{m,i} \tag{2}$$

where $r_{d,i}$ is the annual accumulative probability of detecting violations over the air quality ambient standards for the single monitor i; P_m is the frequency of meteorological scenario m; $T_{m,i}$ is the binary variable used to determine whether the violation is captured by monitor i under meteorological scenario m, such that $T_{m,i} = 1$ if it is captured and $T_{m,i} = 0$ otherwise; M is the total number of meteorological scenarios and I is the total number of monitors.

The concentration measurements at monitor locations were generated using Gaussian puff dispersion model. The pollution episode was considered to be captured if the concentration value exceeded the upper bounds. Then, the plotted profiles of envelopes were overlaid with the monitor locations to determine whether the pollution episode was detected by each given monitor.

r_b is the ratio of the annual accumulative probability of fake sources in the back-calculated source area to the total number of fake sources in the industrial park, which is formulated as Equation (3).

$$r_b = \frac{\sum_{s=1}^{S} r_{b,s}}{S} \tag{3}$$

$$r_{b,\,s} = \sum_{m=1}^{M} P_m N_{m,s} \tag{4}$$

where $r_{b,s}$ is the annual accumulative probability of a single fake source s in the back-calculated source area; P_m is the frequency of meteorological scenario m; $N_{m,s}$ is the binary variable used to determine whether fake source s is located in the source area under meteorological scenario m, such that $N_{m,s} = 1$ if the violation is captured and fake source s is located in the source area, and $N_{m,s} = 0$ otherwise; M is the total number of meteorological scenarios; S is the total number of fake sources in the industrial park.

Equation (3) corresponds precisely to Equation (5), provided that $M = 1$ and $P_m = 1$ when r_b is only calculated under a single

meteorological scenario.

$$r_b = \frac{\sum_{s=1}^{S} N_s}{S} \quad (5)$$

2.1.1. Gaussian puff model

The Gaussian puff model was employed here as the dispersion model in the simulation of pollution detection and source identification, which is one of guideline models for environmental risk assessment on projects (Jiang, 2003; MEPPRC, 2004). The concentration measurement C is expressed as follows:

$$C_i(x,y,z,t) = \frac{Qi}{(2\pi)^{3/2}\sigma_x\sigma_y\sigma_z}\exp\left[-\frac{(x-x_i)^2}{2\sigma_x^2}\right]exp\left[-\frac{(y-y_i)^2}{2\sigma_y^2}\right]\left\{exp\left[-\frac{(z-z_i)^2}{2\sigma_z^2}\right]+exp\left[-\frac{(z+z_i)^2}{2\sigma_z^2}\right]\right\} \quad (6)$$

where C_i is the predicted concentration at the location of (x, y, z) from puff i at (x_i, y_i, z_i); Q_i is the strength of the puff; z_i is the effective stack height of the puff centreline; and σ_x, σ_y, and σ_z represent the dispersion coefficients of the concentration distribution in the x, y and z directions, respectively.

The calculation of the dispersion coefficients under non-low (wind speed ≥ 1.5 m/s), low(1.5 m/s > wind speed ≥ 0.5 m/s) and calm (wind speed < 0.5 m/s) wind conditions were completed according to MEPPRC (1993).

In the forward simulation, real observations of wind speed and wind direction were adopted, and means of temperature gradient—wind speed method (ΔT/U) was employed to determine atmospheric stability classifications (Jiang, 2003). The sounding data from Shanghai radiosounding stations, provided by university of Wyoming (http://weather.uwyo.edu/upperair/sounding.html, Site No. 58362) were used to determine the temperature gradients (Petty, 2008).

2.1.2. Source area analysis

The source area analysis method proposed in our previous work (Huang et al., 2015) was adopted as the method for source identification. Several assumptions are imposed for using this method to estimate the spatial distribution of the potential source:

A1. Although pollution episodes are from a single emission source, some fake sources may be covered by the back-calculated source area. Thus, the results are not sufficient to further deduce the real source from these suspected sources for a pollution episode due to the limited amount of available information.
A2. The emission source is considered to be a point source. Area and volume sources are not considered.
A3. The concentration measurements vary mainly with the source strength and the meteorological conditions.
A4. The emissions may begin a few hours before the detection time of the pollution episode.

The source area can be reconstructed using this method based on meteorological data and concentration measurements. The back-calculated process of the source area analysis is illustrated in Fig. 1.

First, the computation domain is meshed, and the centre of each grid cell is treated as a point emission source. In addition, a reasonable space is provided for each remaining source parameter (such as Q, T, and H). Then, optimal combinations are searched from these spaces at each point. The concentration prediction error at the monitor is evaluated for the searched combinations. A combination of source parameters is considered feasible provided the calculated concentration prediction error is less than the defined error limit. The grid point is accepted as long as a feasible combination is obtained. Finally, the source area is obtained based on optimal *err* values of all grid points.

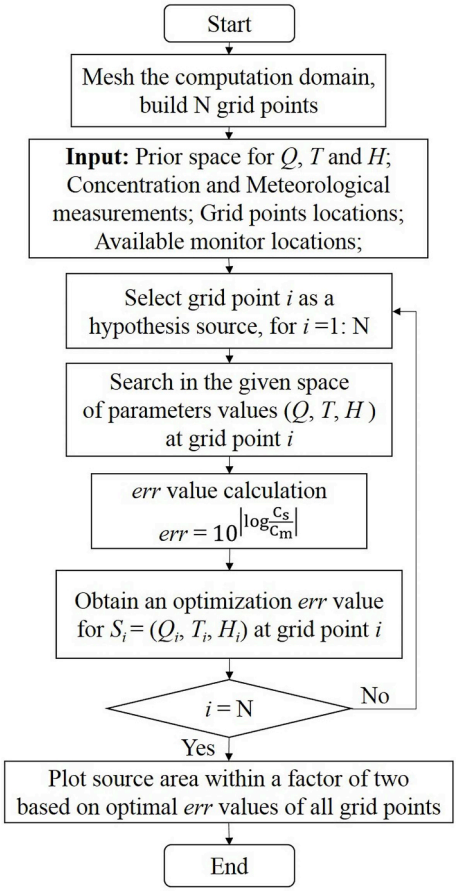

Fig. 1. Computation flow of source area analysis.

In the study, the study area was meshed with a grid interval of 100 m. The upper limit of the release rate was 360 kg h^{-1}, which was determined based on maximum allowable concentration in occupational exposure limits (NHCPRC, 2007) and the peak concentration in whole year at monitors. The emission time was set to be no more than 4 h before the detection time.

The prediction error for each combination of source parameters at each point is calculated using the following equation:

$$\mathrm{err} = 10^{\left|\log\frac{C_s}{C_m}\right|} \quad (8)$$

where C_s and C_m are the simulated and measured concentrations, respectively.

The prediction error in Equation (8) represents the composite level of multiple errors (*i.e.,* measurement error, modelling error, sampling error, source term error and others). These sources of error are difficult to separate in practice. The modelling error of the above dispersion model was directly adopted as the prediction error limit because the sampling and measurement errors are usually involved in the assessment of the modelling error. The error limit was set to a factor of two in this paper. It was considered to be a typical value that reflected a match between measured and simulated concentrations according to Venkatram and Klewicki (2003).

2.2. Data configuration

2.2.1. Real case

An evaluation of surveillance efficiency was performed for the AQMN developing planning of a chemical industrial park in Shanghai, China. This industrial park covered an area of approximately 19 km^2 and included eleven sources of hydrogen sulfide, which are shown in

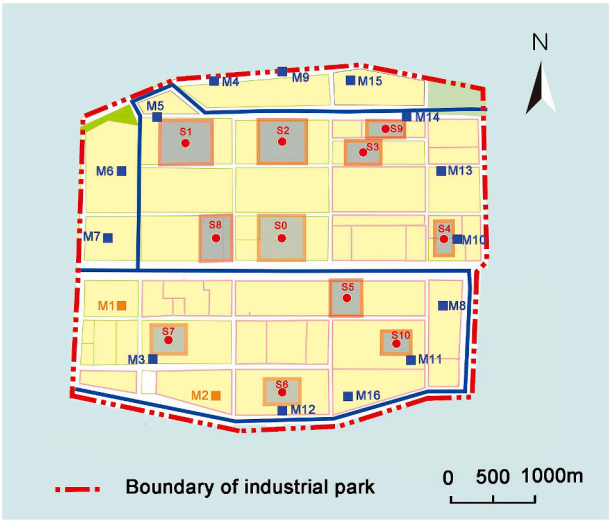

Fig. 2. Arrangements of sources and monitors in the industrial park. The sources (S_0–S_{10}) are denoted by red dots. The orange squares indicate the locations of existing monitors (M_1, M_2). The blue squares indicate the locations of proposed monitors (M_3 - M_{16}). The monitor subscript numbers decreased with the wind direction frequency. (For interpretation of the references to colour in this figure legend, the reader is referred to the Web version of this article.)

Fig. 2. Hydrogen sulfide is a common odour pollutants in industrial parks, especially in chemical parks. The abnormal emission of such odour pollutants has brought serious harm to the industrial park and its surrounding environment. Among these sources, S_0, located at the centre of the industrial park, was the most difficult to exclude from the suspected sources in the back-calculation. Therefore, S_0 was selected as the real source of concern in the evaluation and assumed to be a continuous emitter throughout the whole year, and other sources (S_1–S_{10}) were considered as fake sources. The distances between S_0 and the fake sources (S_1–S_{10}) ranged from 0.75 km (S_8) to 1.94 km (S_4). The emission rate was set to approximately 100 kg h^{-1}.

Two monitoring stations (*i.e.*, M_1 and M_2) were located to the north-northeast and the east-northeast of S_0. Additional stations (i.e., M_3-M_{16}) were located near the industrial park boundary, according to the air quality monitoring programme. The surveillance efficiency was evaluated for different numbers of monitoring stations (2, 4, 6, 8, 10, 12, 14 and 16). The locations of the additional monitors were selected according to the wind direction frequencies. A map of the sixteen monitoring locations is shown in Fig. 2. These monitoring stations were approximately 2 km from S_0. The lower detection limit and background concentration for hydrogen sulfide were set to 0.56 μg m^{-3} (TAPI, 2016) and 13.0 μg m^{-3}, respectively.

Whole-year meteorological measurements at temporal resolution of 1 h were adopted (Fig. 3). Normally, the minimum period that can represent the meteorological fluctuations of a study area is considered to be one year (Arbeloa et al., 1993). The annual frequencies of the sixteen wind directions ranged from 2.18% to 11.32%. The prevailing wind directions were from the north-northeast, northeast and east-northeast, with a combined frequency of approximately 32.21%. The wind frequency from the north-northwest was the lowest, accounting for only 2.18%.

Wind speeds were classified into low wind conditions (0.5–2.0 m/s) and non-low wind conditions (2.0–10.0 m/s). The mean wind speed was 3.49 m/s, and the low wind frequency was 11.74%. Low wind conditions and non-low wind conditions were represented by wind speeds of 1.0 m/s and 2.0 m/s respectively, considering that the results for wind speeds of 2.0–10.0 m/s were very similar. Neutral stability accounted for approximately 50.99% of the whole-year atmospheric conditions.

2.2.2. Test case

A test case was developed to analyse the variation in the efficiency of source identification with distance between sources. In this case, sources were arranged as points on a 3 × 3 grid, as shown in Fig. 4. S_0', located at the centre, was selected as the source of concern. The source grid size increased from 0.2 km to 1.8 km with a step of 0.2 km. A single available monitor was placed at a downwind distance of 2.0 km from S_0', which occurred most often in the real case. Wind speeds of 0.5–10.0 m/s were considered in the test case. The Pasquill stability classification scheme was adopted to divide the atmospheric conditions into six classes (A - F) (MEPPRC, 1991; Jiang, 2003). The western wind was taken as an example. The results for other directions were similar. The probability of source identification was analysed for each existing combination of wind speeds and atmospheric stability. Other parameters were the same as the real case.

3. Results and discussion

3.1. Typical scenarios of pollution detection from the planned monitoring network

The pollution detection scenarios were analysed for eight monitor configurations under different meteorological conditions. The results showed that the number of monitors covered by the envelope (*i.e.,* the number of monitors that detected the pollution episode) was not greater than three for each scenario. The envelope profiles under different wind speeds and atmospheric stabilities when the wind direction was from the west are presented in Fig. 5.

The results showed that M_{10}, located downwind of S_0, was covered by the envelope under low wind conditions. In contrast, M_8 and M_{13}, located in adjacent downwind directions from S_0, might be covered only under the stability classes of A - C and low wind conditions. Thus, the pollution episode was detected by 1–3 monitors when only one monitor was positioned downwind of S_0 for each wind direction, and the 3-monitor case occurred only under the stability classes of A - C and low wind conditions.

Only M_{10}, which was positioned downwind of S_0, was covered by the envelope under the non-low wind conditions. Due to limited space, only the envelope profile under the atmospheric stability of class A is shown in Fig. 5 (b) III. The crosswind span of the envelope decreased with the atmospheric stability class under non-low wind conditions.

Five typical scenarios were identified according to the number of monitors covered by the envelope and were accordingly used for source identification (Fig. 6). *Scenario 1* was the most common situation and is shown in Fig. 6 I. In this scenario, the puffs from source S_0 might reach the monitor directly downwind. In *Scenario 2*, the puffs might also reach a neighbouring monitor in the downwind direction, as shown in Fig. 6 II. There was no monitor directly downwind of S_0 in this scenario. If there were monitors downwind or in the downwind neighbouring areas, the puffs might reach two or three monitors, as in *Scenario 3* (Fig. 6 III) and *Scenario 5* (Fig. 6 V). *Scenario 4* is shown in Fig. 6 IV and represents the monitoring situation in which monitors are located in both of the neighbouring downwind directions but none were downwind. According to the layouts of effective monitoring areas in Fig. 5, *Scenarios 2*–5 might occur under the atmospheric stability classes of A - C and low wind conditions.

Due to the asymmetric distribution of suspected sources, the number of fake sources covered by the source areas differed under various wind directions. The results under some wind directions are taken as examples, as shown in Fig. 7 and Fig. 8. The corresponding r_b values are shown in Fig. 9. The statistics of r_b were obtained assuming the frequency of each meteorological condition to be 1, *i.e.,* using Equation (5).

The variation of back-calculated source area along meteorological conditions in *Scenario 1* is shown in Fig. 7. It was difficult to be excluded from the suspected sources under different meteorological conditions if the fake sources were located upwind or downwind of S_0 because the reconstructed source area extended upwind. The fake sources arranged in other directions but at the same downwind distance were more easily excluded as their distances from the M_1 - S_0 segment increased. The greater the distance, the more easily the fake source was excluded. This is due to the wedge shape of the reconstructed source area.

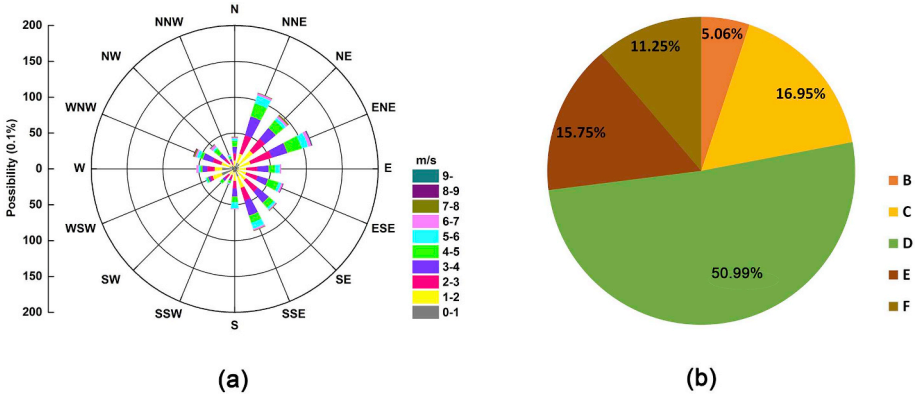

Fig. 3. Meteorological conditions for the study area. (a) Joint frequency distributions of wind direction and speed and (b) frequency distribution of atmospheric stability.

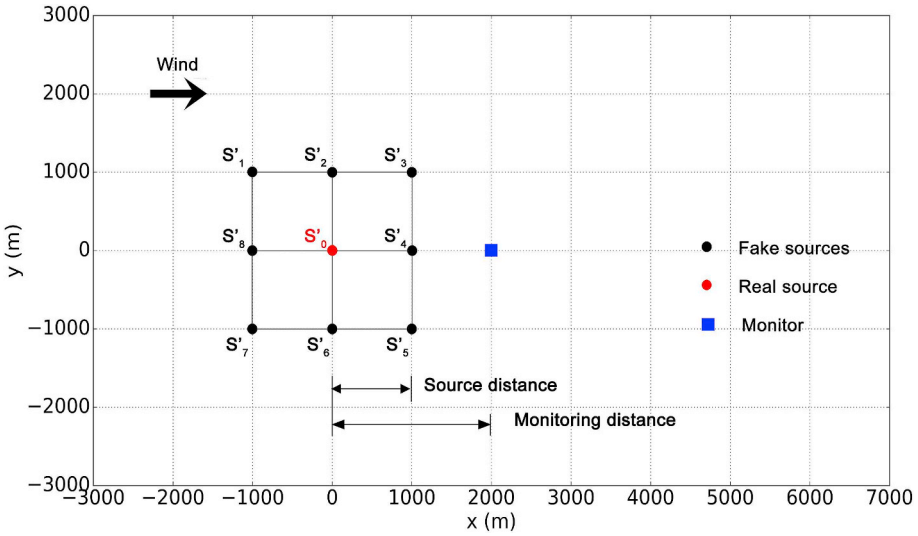

Fig. 4. Illustration of source-monitor configurations for the test case; the concerned source S_0' is located at (0, 0) m. An example of the source map with a 1 km resolution source grid is denoted by black dots. The monitor 2.0 km east of S_0' are denoted by blue squares. (For interpretation of the references to colour in this figure legend, the reader is referred to the Web version of this article.)

The comparison of the results between Fig. 7 (a) and Fig. 7 (b) shows that the crosswind spans of the source area under low wind conditions were much broader than those under non-low wind conditions and that the crosswind span also decreased with changes in the atmospheric stability. Correspondingly, the r_b values (*i.e.* the efficiency of source identification) for *Scenario 1* ranged from 0.00 to 0.60 under non-low wind conditions and from 0.70 to 1.00 under low wind conditions, as shown in Fig. 9.

Ten fake sources were covered completely by the back-calculated source areas in *Scenario 2* to *Scenario 5* under the stability classes of A - B. Due to limited space, only the variation of the back-calculated source area for *Scenario 2* to *Scenario 5* under stability class C are presented in Fig. 8. The results indicated that the shapes of the identified source area in *Scenario 2* and *Scenario 3* were similar, whereas the shape was slightly narrower in *Scenario 4* and *Scenario 5*. The r_b values ranged from 0.90 to 1.00 in *Scenario 2* to *Scenario 5*, as shown in Fig. 9. Noted that the r_b values did not decrease obviously with an increasing number of available monitors in *Scenario 2* to *Scenario 5*. It may be related to the low wind conditions. Thus, the contributions of *Scenario 2* to *Scenario 5* to the back-calculation for a single pollution episode were limited.

3.2. r_d for the planned monitoring network

The calculated r_d increased with the number of monitors in the real case. The r_d value for the two existing monitors (M_1 - M_2) was approximately 0.23, and the value was 1.00 for the sixteen monitors (M_1 - M_{16}). The r_d increased by approximately 3.4 times when the scale of the AQMN expanded seven times. This increase was due to the increasing number of wind directions covered by monitors and was related to the wind frequency characteristics. As shown in Fig. 3 (a), the higher-frequency wind directions accounted for approximately 7.10–11.32%, whereas the lower-frequency wind directions accounted for approximately 2.18–4.50%. Thus, the r_d increased more quickly for M_1 - M_2, M_1 - M_4 and M_1 - M_6 and more slowly for M_1 - M_{12}, M_1 - M_{14}, and M_1 - M_{16} (Fig. 10).

The contributions of *Scenario 1* to *Scenario 5* are also given in Fig. 10. The contributions of one-monitor scenarios (*i.e., Scenario 1* and *Scenario 2*) accounted for more than 97.13% of the r_d value for different AQMN scales and the value of *Scenario 1* accounted for more than 96.67%. Scenarios involving two or three monitors (*Scenario 3* to *Scenario 5*) accounted for approximately 1.23–2.87%. Therefore, the one-monitor scenarios were the most common scenarios of pollution detection in the real case, especially *Scenario 1*.

In these five scenarios, two types of pollution detection are possible for each monitor, *i.e.,* detection at the centreline of the envelope or at the edge of the envelope. Pollution detection at the centreline of the plume for each monitor may have occurred in *Scenario 1, Scenario 3*, and *Scenario 5*, whereas detection at the edge of the envelope might have occurred in *Scenario 2* to *Scenario 5*. The sixteen-monitor

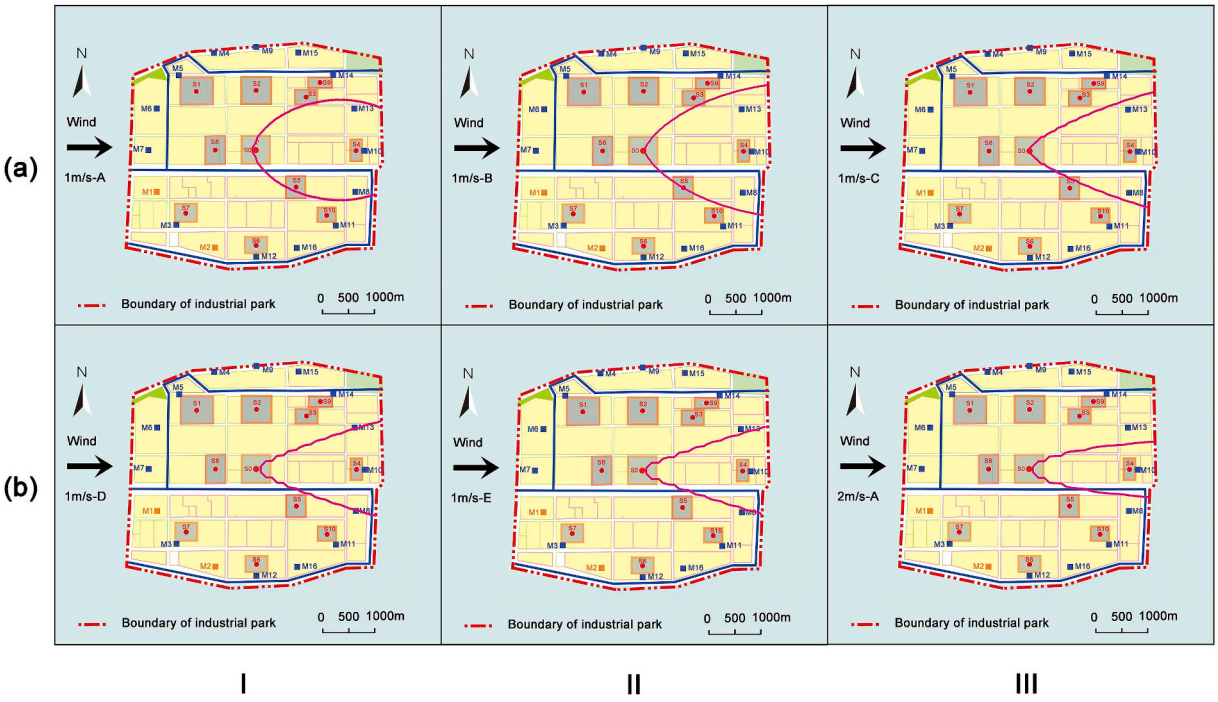

Fig. 5. The layout of effective monitoring areas under different meteorological conditions. The red dots are source locations. The orange squares are the existing monitors for violation detection and the blue squares are the planning monitors. The pink lines are the corresponding plume profiles. (For interpretation of the references to colour in this figure legend, the reader is referred to the Web version of this article.)

configuration (M_1 - M_{16}) is taken as an example. For M_1 - M_{16}, detection at the centreline of the envelope only occurred in *Scenario 1* and *Scenario 5,* whereas detection at the edge of the envelope only occurred in *Scenario 5*. Fig. 11 shows the results of the calculated $r_{d,i}$ for each monitor and the contributions of these two detection types to $r_{d,i}$ for comparison.

The $r_{d,i}$ value was nearly equal to the corresponding wind direction frequency for most monitors, especially for M_9 and M_{15}. The fact that detection at the envelope centreline was the primary contributor to $r_{d,i}$ may be the reason for this. The $r_{d,i}$ values were slightly higher than the corresponding wind frequencies for some monitors due to the increased contribution of detection at the envelope edge. As mentioned above, *Scenario 2* to *Scenario 5* (Fig. 6) occurred only under the stability classes A - C and low wind conditions. The frequency of the stability classes A - C and low wind conditions was greater under winds from the west and west-southwest (W and WSW) than under other wind directions (Fig. 3). Thus, the contribution of detection at the edge of the envelope to $r_{d,i}$ for M_8, M_{13}, M_{10}, and M_{14}, which were located on the edge of the envelope from W and WSW, was higher than that for other monitors.

As discussed above, the puffs from the S_0 emissions was always detected by only one monitor located at the centreline under real meteorological conditions, even though the total number of monitors was sixteen. There was also a low probability that the puffs would also be detected by monitors located at the envelope edge, and this probability was related to the frequency of the occurrence of stability classes A - C and low wind conditions. Accordingly, the number of available monitors for source identification was 1–3 after the pollution episode was detected, and *Scenario 1* was the most common case.

3.3. r_b for the planned monitoring network

The variation in r_b with an increase in the number of monitors is presented in Fig. 12. As shown in Fig. 12, the calculated r_b decreased nonlinearly with the AQMN scale. This indicated that the efficiency of source identification for S_0 emissions increased with the number of monitors. As discussed in the literature (Gao et al., 2010; Rudd et al., 2012), the accuracy of the back-calculation increased with the number of available monitors, which was concluded based on the back-calculation results of a pollution episode. While Fig. 12 shows the annual statistical results of the back-calculation based on long-term measurements. As mentioned above, 1–3 monitors might be used for source identification, but only one monitor was available in most cases.

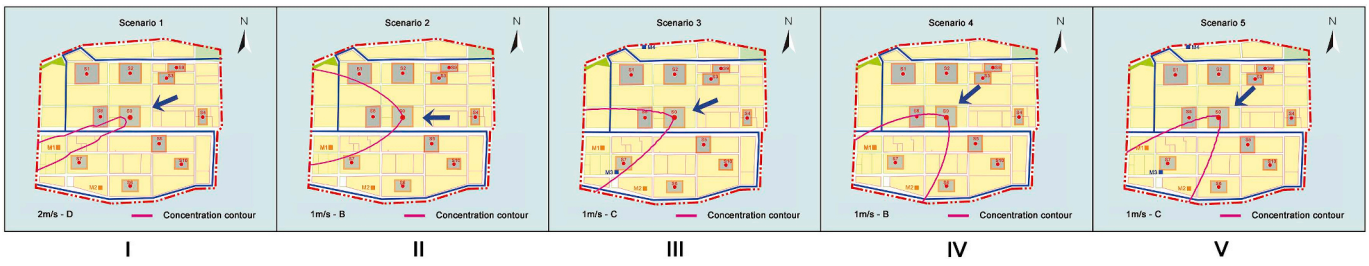

Fig. 6. Typical scenarios layouts of monitor covered by the plume. The pink curves are the plume profiles. The wind directions are marked with blue arrows. I and II indicate the scenario in which only one monitor is covered by the plume; III and IV indicate the scenario in which two monitors are covered by the plume; V indicates the scenario in which three monitors are covered by the plume. (For interpretation of the references to colour in this figure legend, the reader is referred to the Web version of this article.)

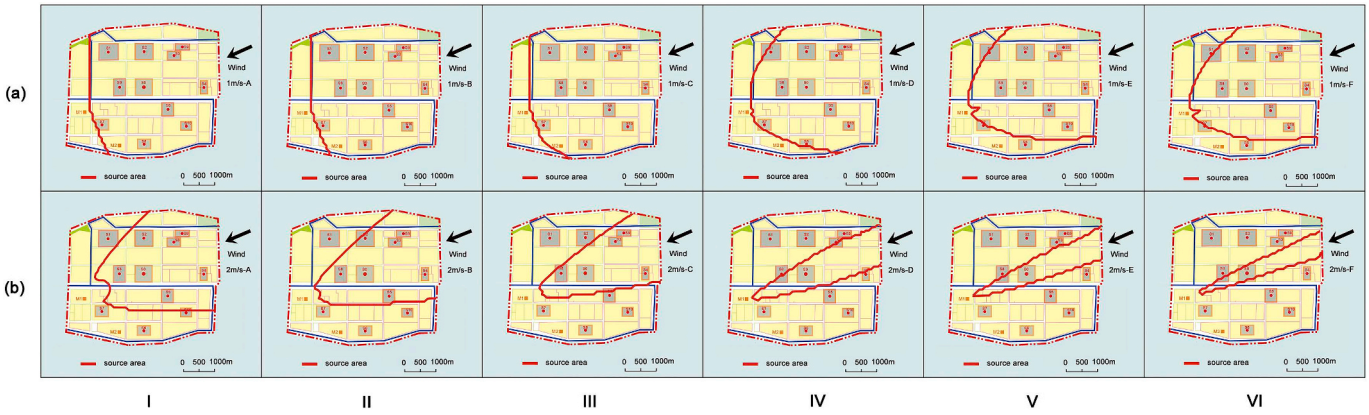

Fig. 7. Layout of back-calculated source area in *Scenario 1* under different meteorological conditions. (a) Under low wind conditions and (b) under non-low wind conditions.

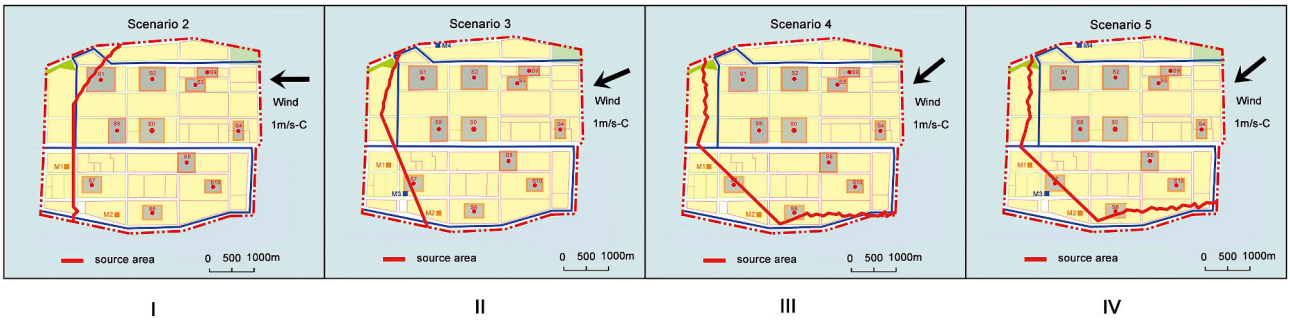

Fig. 8. Layout of back-calculated source area in *Scenario 2* - *Scenario 5* under different meteorological conditions. (a) *Scenario 2* - *Scenario 4* and (b) *Scenario 5*.

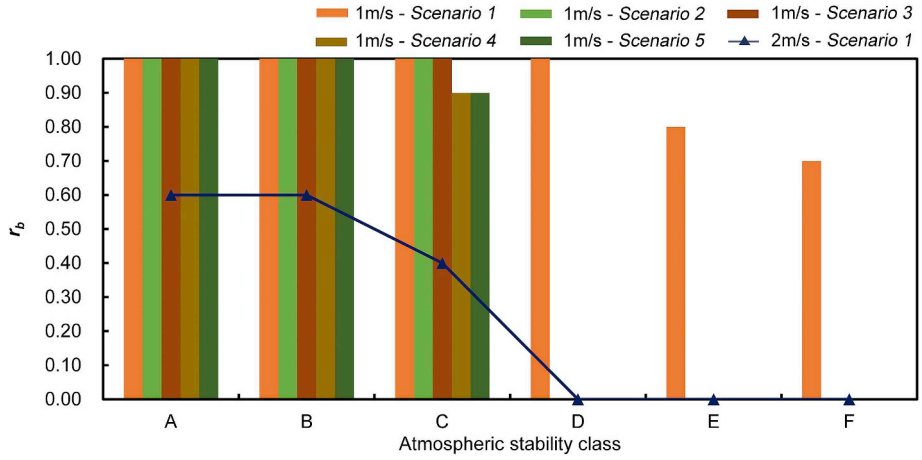

Fig. 9. r_b distribution for *Scenario 1* - *Scenario 5* under different meteorological conditions.

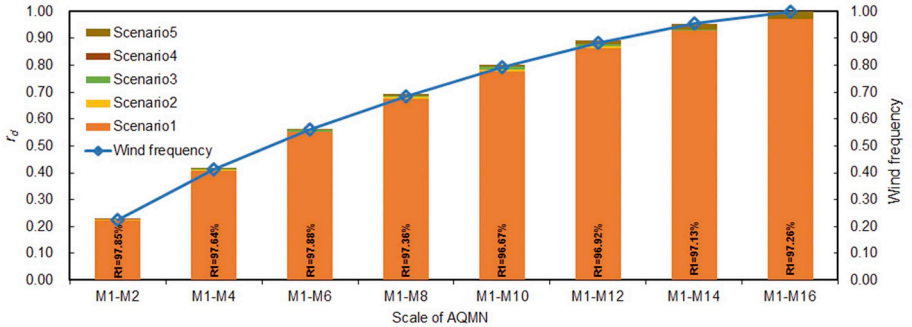

Fig. 10. r_d variation with AQMN scale and wind frequency from S_0 to the deployed monitors. R_1 indicates the contribution ratio of *Scenario1* to r_d. M_1 - M_2 indicates M_1 and M_2, and M_1 - M_{16} indicates sixteen monitors.

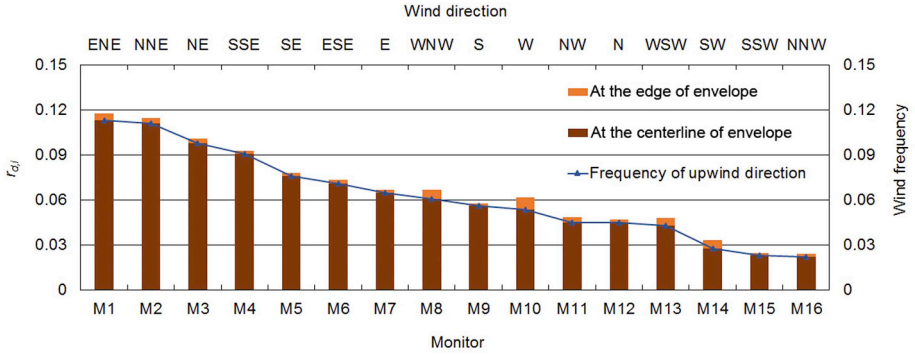

Fig. 11. $r_{d,i}$ for M_i and the frequencies of winds blowing from S_0 to M_i.

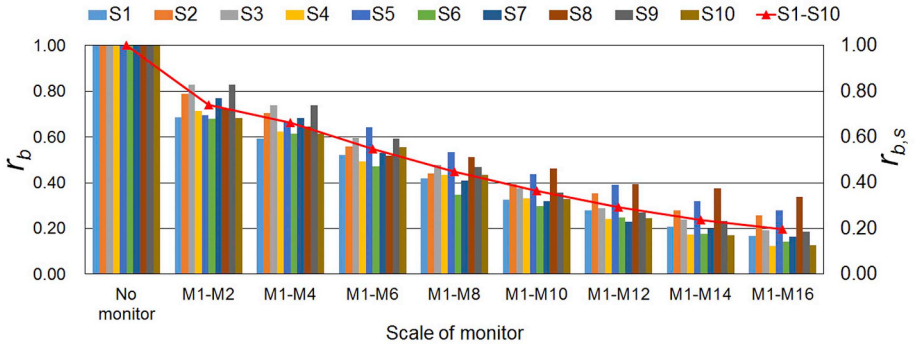

Fig. 12. r_b variation with AQMN scale and $r_{b,s}$ variation for each fake source.

Meanwhile, the contributions of *Scenario 2* to *Scenario 5* to the back-calculation for a single pollution episode were limited. Thus, the main reason for the increased efficiency of source identification in the real case was not an increase in the number of monitors in the back-calculation for each pollution episode but the increased probability of pollution detection.

The results of r_b and $r_{b,s}$ with no monitors are also given in Fig. 12 for comparison. All fake sources (S_1 - S_{10}) cannot be separated from the suspected source when no monitors are available, *i.e.,* $r_{b,s}$ was 1 for each fake source. The r_b value for the two existing monitors (M_1 - M_2) was approximately 0.74. This indicated that some fake sources may not be covered by the source area in the back-calculation for some pollution episodes. The r_b was relatively high for M_1 - M_2, because $r_{b,s}$ was still 1 for the pollution episodes under some wind directions when only M_1 and M_2 were deployed. Pollution episodes under more wind directions can be captured with a greater number of monitors, and then more and more fake sources can be excluded by the source area analysis. Thus, the calculated r_b decreased with an increasing number of monitors. r_b was not lower than 0.20 for M_1 - M_{16}, though r_d have been up to 1. Because there was still a low probability for M_1 - M_{16} that a pollution episode could be detected by multiple monitors under the meteorological characteristics of this case.

The $r_{b,s}$ variation with the number of monitors differed for each fake source, as shown in Fig. 12. The $r_{b,s}$ values for S_3 and S_9 were higher than those for other fake sources when only M_1 and M_2 were deployed. This was because the downwind distances from S_0 to these two sources were greater and the distances from these two sources to the M_1 - S_0 and M_2 - S_0 segments were shorter than those for other sources. The $r_{b,s}$ decreased for each fake source when M_3 and M_4 were added, and the value decreased more slowly for S_5 than for other sources for the same reason. The comparison between the results of M_1 - M_2 and those of M_1 - M_4 showed that the relative location relationships between the fake sources and the envelope centreline were different in different back-calculation scenarios when monitors were added under different wind directions. A fake source might be easy to be excluded in the M_1 - M_4 scenario but difficult to be excluded in the M_1 - M_2 scenario. Thus, the $r_{b,s}$ variation was related to the source distributions and the frequencies of meteorological conditions in the real case. Overall, the $r_{b,s}$ value decreased with the number of monitors for each fake source (sometimes quickly, sometimes slowly).

The $r_{b,s}$ value was not obviously related to the distance from S_s to M_i - S_0 when sixteen monitors (M_1 - M_{16}) were deployed, due to the superposition analysis of the back-calculated source area under sixteen directions. Instead, the correlation between the $r_{b,s}$ value and the distance from S_s to S_0 became significant for M_1 - M_{16}. For example, the $r_{b,s}$ values of M_1 - M_{16} for S_2, S_5 and S_8 were higher than those of the other fake sources, which were closer to the real source S_0; The values for S_4 and S_{10} were lower, which were farther from the real source S_0. The fake sources S_5 and S_{10} were located in the same direction, but the former was closer to S_0 (Fig. 2). The $r_{b,s}$ value of M_1 - M_{16} for S_5 was more than two times that for S_{10}.

3.4. Discussion

Detection of pollution episodes under different wind directions was guaranteed when there was one monitor for each wind direction, but the number of monitors available for source identification was still not enough. Due to the limited crosswind span of the envelope, pollution episodes were difficult to be detected by the monitors located at the envelope edge under most meteorological conditions (Fig. 5). As shown in Fig. 10, the contribution rates of *Scenario 2* to *Scenario 5* were no higher than 3.33%. Additionally, the back-calculation performances of *Scenario 2* to *Scenario 5* were poor (Fig. 9). Thus, adding monitors at the envelope edge to provide more measurements for source identification is not recommended. Instead, positioning monitors at the centreline is preferable for long-term surveillance of air pollution episodes from a certain wind direction.

The fake sources that were close to the real source were difficult to be excluded from the suspected sources. Considering that pollution sources in the real case were distributed asymmetrically, a test case was

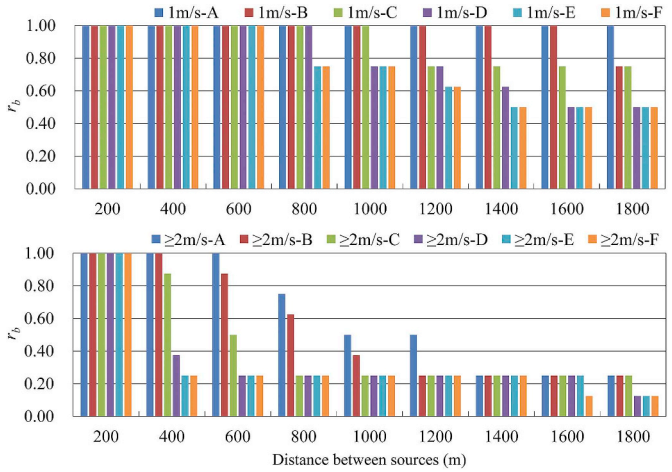

Fig. 13. r_b distribution for different distances between sources under different meteorological conditions. (a) Under low wind conditions and (b) under non-low wind conditions.

constructed to examine the impact of the distance between sources on r_b. The r_b variation with distance between sources is presented in Fig. 13. The statistics were completed under the assumption that the frequency of each meteorological condition was 1, *i.e.,* using Equation (5). The results showed that the r_b value decreased with increasing distance between sources. The r_b value decreased with increasing distance between sources more slowly under low wind conditions than under non-low wind conditions and decreased more quickly with improving atmospheric stability. The r_b values were always 1 under different meteorological conditions when the distance between sources was 0.2 km, which represented eight fake sources were covered by the source area. Thus, a fake source within 0.2 km of the real source could not be separated from the suspected sources in real pollution episodes.

In the evaluation, simulated concentrations generated by Gaussian puff dispersion model were used as ambient concentration measurements. Because historical emissions information is unavailable in real case, even though there were historical observations from two existing stations. It is not enough to support the evaluation of pollution detection efficiency in this case. In addition, more other stations which were still under construction, measurements from which were uknown. Thus, synthetic data was used to do unified evaluation for both the existing and planned stations. The real measurements are not consistent with the simulated concentrations due to the impact of multiple errors such as monitoring error and simulating error. Therefore, the discrepancies between measurements and simulation should be further considered in real scenario.

4. Conclusions

A developing planning of AQMN in a real chemical industrial park was evaluated in this study. This is a boundary-type construction planning of AQMN, in which stations were planned to be placed at different directions on the boundary of this park. The planning was generated to ensure the better surveillance of pollutants from the park to outside. The result of surveillance efficiency evaluation showed that efficiency of pollution detection increased almost linearly with the number of monitors. Meanwhile, there is usually only one monitor (located around the envelope centreline) which can provide information on the ambient concentration enhancement resulted from a single pollution episode. There was a low probability that a pollution episode could be detected by multiple monitors under the meteorological characteristics of this case. Thus, source identification efficiency was not lower than 0.20 on the average annual scale, though pollution detection efficiency may be up to 1.00. It means that back-calculation of S_0 emission would be interfered by two fake sources on average.

The low efficiency of source identification was not only related to the limited available monitors for each pollution episode, but also related to sensitivity to meteorological conditions, the number of monitors and the distance between sources. According to the sensitivity analysis of source identification efficiency, r_b decreased with the distance between sources, indicating that fake sources become more difficult to be separated from the real source with decreasing distance between the sources. Fake sources located at distances of less than 0.2 km from real source cannot be separated from suspected sources under different meteorological conditions.

The boundary-type AQMN concerned in this study is always the most basic part of a completed AQMN, which can ensure satisfying efficiency of pollution detection, but comprehensive efficiency of back-calculation is relatively low. It is also the functional limitation of boundary-type AQMN. How to arrange optimally more monitoring stations or mobile monitoring equipments inside the park would be taken into account in subsequent studies, considering multiple real sources' arrangements and local meteorological characteristics for further improving source identification efficiency.

Declaration of interests

The authors declare that they have no known competing financial interests or personal relationships that could have appeared to influence the work reported in this paper.

Acknowledgements

This work was supported by the project of Science and Technology Commission of Shanghai Municipality (Grant no.15DZ1205303).

Appendix A. Supplementary data

Supplementary data to this article can be found online at https://doi.org/10.1016/j.atmosenv.2019.116874.

References

Adams, M.D., Kanaroglou, P.S., 2013. Optimized monitor reduction for an industrial air pollution monitoring network. In: Proceedings of the 13th International Conference on Environmental Science and Technology, Athens, Greece, 5-7 September 2013.
Allen, C.T., Young, G.S., Haupt, S.E., 2007. Improving pollutant source characterization by better estimating wind direction with a genetic algorithm. Atmos. Environ. 41 (11), 2283–2289.
Arbeloa, F.J.S., Caseiras, C.P., Andrés, P.M.L., 1993. Air quality monitoring: optimization of a network around a hypothetical potash plant in open countryside. Atmos. Environ. Part A. general Topics 27 (5), 729–738.
Cai, T.X., Wang, S.J., Xu, Q., Ho, T.C., 2013. Proactive abnormal emission identification by air-quality-monitoring network. Ind. Eng. Chem. Res. 52 (26), 9189–9202.
Chow, F.K., Kosović, B., Chan, S., 2008. Source inversion for contaminant plume dispersion in urban environments using building-resolving simulations. J. Appl. Meteorol. Climatol. 47 (6), 1553–1572.
Efthimiou, G.C., Kovalets, I.V., Venetsanos, A., Andronopoulos, S., Argyropoulos, C.D., Kakosimos, K., 2017. An optimized inverse modelling method for determining the location and strength of a point source releasing airborne material in urban environment. Atmos. Environ. 170, 118–129.
Flesch, T.K., Wilson, J.D., Harper, L.A., 2005. Deducing ground-to-air emissions from observed trace gas concentrations: a field trial with wind disturbance. J. Appl. Meteorol. 43 (43), 487–502.
Gao, Z.L., Desjardins, R.L., Flesch, T.K., 2010. Assessment of the uncertainty of using an inverse-dispersion technique to measure methane emissions from animals in a barn and in a small pen. Atmos. Environ. 44 (26), 3128–3134.
Haupt, S.E., Young, G.S., Allen, C.T., 2007. A genetic algorithm method to assimilate sensor data for a toxic contaminant release. J. Comput. 2 (6).
Hosseini, B., Stockie, J.M., 2016. Bayesian estimation of airborne fugitive emissions using a Gaussian plume model. Atmos. Environ. 141, 122–138.
Huang, Z.H., Wang, Y., Yu, Q., Ma, W.C., Zhang, Y., Chen, L.M., 2015. Source area identification with observation from limited monitor sites for air pollution episodes in industrial parks. Atmos. Environ. 122, 1–9.
Jiang, W., 2003. Air Pollution Meteorology. Nanjing University Press, Nanjing, China, pp. 124–125.
Khlaifi, A., Ionescu, A., Candau, Y., 2009. Pollution source identification using a coupled diffusion model with a genetic algorithm. Math. Comput. Simulat. 79 (12), 3500–3510.

Kovalets, I.V., Andronopoulos, S., Venetsanos, A.G., Bartzis, J.G., 2011. Identification of strength and location of stationary point source of atmospheric pollutant in urban conditions using computational fluid dynamics model. Math. Comput. Simulat. 82 (2), 244–257.

Kumar, P., Feiz, A.A., Ngae, P., Singh, S.K., Issartel, J.P., 2015. CFD simulation of short-range plume dispersion from a point release in an urban like environment. Atmos. Environ. 122, 645–656.

Kumar, P., Singh, S.K., Feiz, A.A., Ngae, P., 2016. An urban scale inverse modelling for retrieving unknown elevated emissions with building-resolving simulations. Atmos. Environ. 140, 135–146.

Long, K.J., Haupt, S.E., Young, G.S., 2010. Assessing sensitivity of source term estimation. Atmos. Environ. 44 (12), 1558–1567.

Ma, D.L., Deng, J.Q., Zhang, Z.X., 2013. Comparison and improvements of optimization methods for gas emission source identification. Atmos. Environ. 81 (2), 188–198.

Ma, D.L., Zhang, Z.X., 2016. Contaminant dispersion prediction and source estimation with integrated Gaussian-machine learning network model for point source emission in atmosphere. J. Hazard Mater. 311, 237–245.

MEPPRC (Ministry of Environmental Protection of the People's Republic of China), 1991. Technical methods for making local emission standards of air pollutants (GB/T3840-91). Available from: http://kjs.mep.gov.cn/hjbhbz/bzwb/other/qt/199206/t19920601_67580.htm (Chinese).

MEPPRC (Ministry of Environmental Protection of the People's Republic of China), 1993. Technical Guidelines for Environmental Impact Assessment Atmospheric Environment (HJ/T2.2-1993). (Chinese).

MEPPRC, 2004. Technical guidelines for environmental risk assessment on projects (HJ/T 169-2004). Available from: http://kjs.mep.gov.cn/hjbhbz/bzwb/other/pjjsdz/200412/W020110127329297430823.pdf (Chinese).

Najafi, S.K., Gilbert, E., 2003. USE OF REAL-TIME MEASUREMENTS FOR ESTIMATING RELEASE RATE. In: In Institution of Chemical Engineers Symposium Series, vol. 149. pp. 155–172.

NHCPRC (National Health Commission of the People's Republic of China), 2007. Occupational exposure limits for hazardous agents in the workplace, Part 1: chemical hazardous agents. http://117.128.6.9/cache/www.nhc.gov.cn/wjw/pyl/200704/38838/files/5eb946b479124c32a6ebb8c49f483c24.pdf?ich_args2=462-15143507024090_dbddd9ca78541d531c09f514054ebfeb_10001002_9c896129d4c2f1d0933d518939a83798_6267ff2837eec8e30b818e3c10d486d6.

Petty, G.W., 2008. A first course in atmospheric thermodynamics. Sundog Pub., Madison, WI, USA, pp. 337.

Pope, R., Wu, J.G., 2014. A multi-objective assessment of an air quality monitoring network using environmental, economic, and social indicators and gis-based models. J. Air Waste Manag. Assoc. 64 (6), 721–737.

Rodriguez, L.M., Haupt, S.E., Young, G.S., 2011. Impact of sensor characteristics on source characterization for dispersion modeling. Measurement 44 (5), 802–814.

Rudd, A.C., Robins, A.G., Lepley, J.J., Belcher, S.E., 2012. An inverse method for determining source characteristics for emergency response applications. Boundary-Layer Meteorol. 144 (1), 1–20.

Sharan, M., Singh, S.K., Issartel, J.P., 2012. Least square data assimilation for identification of the point source emissions. Pure Appl. Geophys. 169 (3), 483–497.

Singh, S.K., Rani, R., 2014. A least-squares inversion technique for identification of a point release: application to fusion field trials 2007. Atmos. Environ. 92, 104–117.

Singh, S.K., Sharan, M., Issartel, J.P., 2015. Inverse modelling methods for identifying unknown releases in emergency scenarios: an overview. Int. J. Environ. Pollut. 57 (1/2), 68–91.

Singh, S.K., Kumar, P., Turbelin, G., Rani, R., 2017. Uncertainty characterization in the retrieval of an atmospheric point release. Atmos. Environ. 152, 34–50.

TAPI (Teledyne API), 2016. User MANUAL MODEL T101 UV FLUORESCENCE H2S ANALYZER. Available from: http://www.teledyne-api.com/prod/Downloads/07266C%20-%20T101%20Manual.pdf#search=Operation%20manual.

Turbelin, G., Singh, S.K., Issartel, J.P., 2014. Reconstructing source terms from atmospheric concentration measurements: optimality analysis of an inversion technique. J. Adv. Model. Earth Syst. 6 (4), 1244–1255.

Venkatram, A., Klewicki, J., 2003. Validation of Concentrations Estimated from Air Dispersion Modeling for Source-Receptor Distances of Less than 100 Meters. California. California Air Resources Board, Research Division, Sacramento.